Danish Meteorological Institute
Ministry of Climate and Energy

Scientific Report 12-01

An upper-tropospheric clear and cloudy air turbulence index in DMI-HIRLAM

Niels Woetmann Nielsen and Claus Petersen

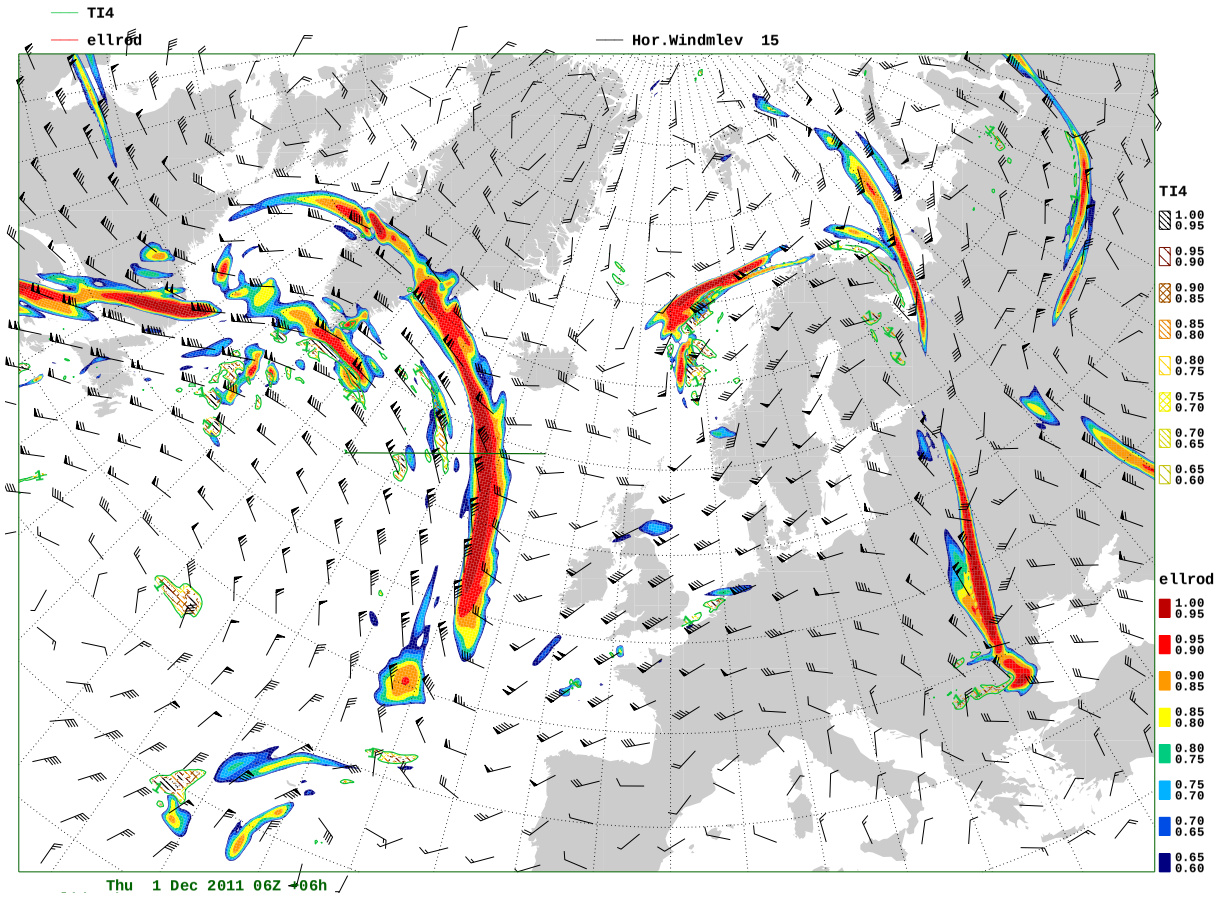

Colophone

Serial title:
Scientific Report 12-01

Title:
An upper-tropospheric clear and cloudy air turbulence index in DMI-HIRLAM

Subtitle:

Authors:
Niels Woetmann Nielsen and Claus Petersen

Other Contributers:

Responsible Institution:
Danish Meteorological Institute

Language:
English

Keywords:
Turbulent Kinetic Energy (TKE), Turbulent potential energy (TPE),Clear Air Turbulence (CAT), Cloudy Air Turbulence (CAT),deformation, shear deformation, stretching deformation, divergence, relative vorticity, absolute vorticity,shear production, buoyancy production/destruction, frontogenesis function, turbulence index

Url:
www.dmi.dk/dmi/sr12-01

ISSN:
******

ISBN:
978-87-7478-608-5

Version:
1

Website:
www.dmi.dk

Abstract

Two dimensionless clear air turbulence indices valid for midlatitude synoptic-scale flow in the upper troposphere are developed. One index ($TI3$) is applicable to flow with high resultant horizontal deformation, and the other ($TI4$) is applicable to flow with low resultant horizontal deformation. The regions depicted by the indices generally have little or no overlap. It is argued that the $TI3$ type of turbulence mainly originates from inflection point instability in the horizontal flow, while the $TI4$ type mostly originates from Kelvin-Helmholtz instability triggered by gravity wave activity in unbalanced flow. The $TI3$ and $TI4$ indices mainly point to regions on the cyclonic and anticyclonic side of jet streams, respectively. The $TI3$ index is related to a widely applied dimensional index in numerical weather forecasting. The latter index is basically the product of the resultant horizontal deformation and the magnitude of the vertical wind shear (Ellrod and Knapp 1992). $TI3$ differs from the former index by being an inverse function of the static stability of the air. $TI4$ can be considered as a dimensionless alternative to a horizontal divergence trend term proposed by Ellrod and Knox (2005). The nondimensional indices depend on the same parameters, with the exception that $TI3$ in addition depends on the vertical wind shear and $TI4$ on the planetary and relative vorticity. $TI3$ and $TI4$ are post-processed experimental products in the operational weather prediction model system at the Danish Meteorological Institute and so far no verification against clear air turbulence reports has been possible.

1: Introduction

Turbulence is almost always present in the atmospheric boundary layer (ABL), but it may also occur above the ABL, in particular in connection with straight and curved jet streams in the upper troposphere. The latter type of turbulence is called clear-air turbulence (CAT), although it can occur in cloudy conditions as well (e.g. Ellrod and Knox 2005).

Generation of turbulence is directly or indirectly due to various kinds of instabilities that may develop in the atmosphere. In some cases CAT can be generated by shear instability without involvement of other instability mechanisms. In other cases it probably develops from shear instability due to local enhancement of vertical velocity shear by gravity waves generated by other types of instabilities among which inertial instability (e.g. Ellrod and Knox 2005) and gravity waves generated by deep moist convection (DMC) (e.g. Kaplan et al. 2005) have been connected with CAT. Also regions with substantial enhancement of vertical and horizontal wind shear due to outflow near the tropopause from large DMC systems have been mentioned as possible CAT-regions (Fritsch and Maddox 1981).

In the present report the focus is on CAT either generated directly from shear instability or by shear instability triggered by gravity waves generated by inertial instability. This means that CAT generated by orography- induced breaking gravity waves or by DMC, including slantwise convection in symmetric unstable flow conditions, is not considered.

In the course of time CAT has been responsible for a large number of aircraft damages and personal injuries. Efforts have therefore been spend on developing reliable diagnostic tools that are able to highlight regions where outbreaks of CAT are likely to occur. It has turned out to be a difficult task to develop such tools with high reliability, partly because CAT is highly transient and tends to occur on horizontal scales down to less than 1 km (Kaplan et al. 2005), and partly because different mechanisms are able to trigger CAT.

Two dimensionless diagnostic CAT indices suitable for midlatitude synoptic-scale flow are proposed and discussed in the present report. It is shown that the CAT risk regions localized by the two

methods tend to have little overlap. The first index, named $TI3$, points to an environment with a risk of CAT related directly to shear instability. This index depends on static stability and is further closely related to the two-dimensional frontogenesis function. It therefore mainly points to regions with strong horizontal and vertical wind shear collocated with weak static stability. The second index, named $TI4$, points to regions, where there is a risk of CAT either triggered by gravity waves generated by inertial instability or directly as result of shear instability due to a large vertical wind shear. In the Northern Hemisphere high values of $TI4$ occur where the absolute vorticity becomes numerically small. The absolute vorticity η is the sum of relative vorticity ζ and planetary vorticity f. On synoptic scales small numerical values of η ($<< f$) may occur in jet streams on their anticyclonic sides.

The $TI3$ index is related to a widely applied dimensional CAT index containing the product of resultant horizontal deformation (DEF) and the magnitude of the vertical wind shear $S = |\partial \mathbf{V}/\partial z|$ (Ellrod and Knapp 1992), but $TI3$ is novel, by having a dependence on static stability, defined as $N^2 = (g/\theta_v)\partial\theta_v/\partial z$, where N is the Brunt-Väisälä frequency and θ_v is the virtual potential temperature. A dependence of $TI3$ on N^2 appears plausible, since it is expected that turbulent kinetic energy at a given vertical wind shear decreases with increasing N^2, as discussed in Section 3. Furthermore, inclusion of N^2 as a parameter in $TI3$ also means that this index can be written in terms of the gradient Richardson number $Ri = N^2/S^2$. Ri appears in the criterion for Kelvin-Helmholtz instability (vertical wind shear instability). The latter is considered as the key instability mechanism by which CAT is generated. The $TI4$ index is related to the horizontal divergence (DIV) trend term proposed by Ellrod and Knox (2005) in the sense that both terms mainly points to regions where inertial instability can occur, i.e to the anticyclonic side of jet streams with anticyclonic curvature. Knox et al. (2008) showed that the divergence trend term is related to $\partial DIV^2/\partial t$ in the Lighthill-Ford shallow-water wave equation for a stably stratified rotating flow. For synoptic-scale midlatitude flow they found that $\partial DIV^2/\partial t$ was the second largest "gravity wave radiation term" in the wave equation. It must be emphasized that outbreaks of CAT occur on sub-synoptic scales, often in domains with horizontal scales from less than 1 km to about 100 km. Therefore, the CAT indices depict synoptic-scale regions within which there is a risk for outbreaks of CAT on a smaller scale, much in the same way as certain synoptic-scale patterns can depict regions with enhanced risk of DMC.

Since shear instability plays a fundamental role in development of CAT, and in stably stratified air is the only production term for turbulent kinetic energy, the following Section 2 briefly presents some fundamentals of the turbulent kinetic and potential energy equations. In Section 3 the relation between horizontal and vertical wind shear instability and CAT is considered. Flow with high resultant horizontal deformation is treated in Section 4 and a nondimensional CAT index, $TI3$, for this flow type is presented in Section 5. Flow with low resultant horizontal deformation is discussed in Section 6, and is in Section 7 the basis for the presentation and discussion of a CAT index, $TI4$, applied for the latter flow type. A case study, illustrating typical patterns of $TI3$ and $TI4$ is presented in Section 8. Finally, conclusions together with a brief summary are given in Section 9.

2: Turbulent kinetic and potential energy

A useful conception of turbulence can be gained from the budget equations for turbulent kinetic and potential energy. Mean turbulent kinetic energy per unit mass (TKE) is defined as $E_K = \overline{\mathbf{V'} \cdot \mathbf{V'}}/2$, where $\mathbf{V'} = \mathbf{V} - \overline{\mathbf{V}}$ is the deviation of the instantaneous wind velocity $\mathbf{V}$ from its mean value $\overline{\mathbf{V}}$. In practice the average is usually over time, and the averaging time must be short enough to retain diurnal and synoptic variations of the atmospheric state and longer than a typical time scale for the turbulent fluctuations. In vector form the TKE budget is (e.g. Garrat, 1992)

$$\frac{\partial E_K}{\partial t} = -\overline{\mathbf{V}} \cdot \nabla E_K - \overline{\mathbf{V'} \cdot (\mathbf{V'} \cdot \nabla \overline{\mathbf{V}})} + \beta \overline{\mathbf{V'} \theta_v'} \cdot \mathbf{k} - \nabla \cdot \overline{(e_k + p'/\rho)\mathbf{V'}} + \nu \overline{\mathbf{V'} \cdot \nabla^2 \mathbf{V'}}, \quad (1)$$

where primed variables are differences between instantaneous and mean values $\beta = g/\overline{\theta_v}$ is the buoyancy parameter, g is gravity, $\mathbf{k}$ is the vertical unit vector and $e_k = \mathbf{V'} \cdot \mathbf{V'}/2$ is the instantaneous TKE. From a generation and consumption of TKE point of view the relevant terms on the right hand side (r.h.s.) of (1) are the second, third and last term. The latter is dissipation of TKE by molecular friction. It is always a sink term for TKE ($\mathbf{V'}$ is negatively correlated with the Laplacian of $\mathbf{V'}$, since the latter tends to be proportional to $-\mathbf{V'}$). In the dissipation term ν is the kinematic viscosity of air. The second term can be rewritten as

$$-(\overline{u'\mathbf{V'}}\nabla\overline{u} + \overline{v'\mathbf{V'}}\nabla\overline{v} + \overline{w'\mathbf{V'}}\nabla\overline{w}). \quad (2)$$

All the terms in (2) except the "diagonal" terms $\overline{u'u'}\frac{\partial \overline{u}}{\partial x}$, $\overline{v'v'}\frac{\partial \overline{v}}{\partial y}$ and $\overline{w'w'}\frac{\partial \overline{w}}{\partial z}$ are always positive (or zero in the trivial case of no mean velocity gradients). These terms (six in total) are therefore called velocity shear production terms. In the atmosphere significant velocity shear is often present near the bottom boundary of the atmosphere due to the no slip condition at this boundary. Vertical wind shear production of TKE therefore usually contributes to turbulence in the atmospheric boundary layer (ABL), i.e. the layer at the bottom of the atmosphere influenced by surface friction and time varying conditions at the surface and above the ABL. In the ABL the vertical shear of the horizontal wind is usually much larger than the horizontal shear. In fact the contribution to turbulence from the horizontal shear is neglected in many applications.

Basically due to the rotation of the Earth significant velocity shear, both horizontal and vertical, can also be created above the ABL. In the troposphere the most important shear regions above the ABL are located near meandering jet cores in the upper troposphere. These jets are often classified into arctic, polar and subtropical jets, each associated with a significant and rather abrupt lowering of tropopause-height in transversing from the warm to the cold side of the jet. The air is normally stably stratified in the strong shear regions connected with the upper-tropospheric jets. Under these circumstances the mean virtual potential temperature ($\overline{\theta}_v$) in the atmosphere increases with height. Therefore rising turbulent eddy motion ($w' > 0$) tends to carry air parcels with lower $\overline{\theta}_v$ than outside the parcel. At some arbitrary level (within the region of turbulence) this results in $\theta_v' < 0$ when parcels from below arrive at this level. In the same way sinking eddy motion ($w' < 0$) leads to $\theta_v' > 0$ when parcels arrive at the fixed level from above. This means that the buoyancy term, which is the third term on the r.h.s. of (1), is negative in presence of turbulence if the atmosphere is stably stratified. In other words, the buoyancy term is a sink term for TKE in stable stratification. The just described process is thermal indirect by converting TKE into turbulent potential energy E_P, given by $E_P = \frac{1}{2}(\beta/N)^2\overline{\theta_v'^2}$.

It is possible to derive an equation for E_P similar to the TKE equation (e.g. Zilitinkevich et al. 2007). This turbulent potential energy equation (TPE) also contains the buoyancy production/consumption term, but with opposite sign of that in the TKE equation. The total turbulent energy is defined as $E = E_K + E_P$, and in the total turbulent energy (TTE) budget equation for E obtained by adding the TPE and TKE equations, the buoyancy terms therefore cancel, leaving the velocity shear production as the only production term for E.

3: Shear instability

It becomes clear from the discussion above that only the velocity shear production term in (1) has the potential to generate total turbulent energy E. In stably stratified air the buoyancy consumption term is a destruction term for E_K in the TKE equation, but appears as a buoyancy production term

for E_P in the TPE equation and vice versa if the air is unstably stratified. Generation of E occurs in a process named shear instability, consisting of horizontal and vertical shear instability. A necessary but insufficient condition for horizontal shear instability is that a relative maximum in the vertical component of shear vorticity is present in the flow. Such a maximum is also an inflection point in the horizontal wind profile, that is a point where the second horizontal derivative of the horizontal wind speed changes sign, and for this reason horizontal shear instability is also named inflection point instability.

Due to presence of negative buoyancy in stably stratified air vertical shear instability does not require an inflection point (local maximum in horizontal shear vorticity) in the vertical profile of the horizontal wind. Instead a necessary but insufficient condition for vertical shear instability, also named Kelvin-Helmholtz instability (K-H instability), is that $Ri < Ri_* = 0.25$, where Ri_* is the critical Richardson number. The criterion for K-H instability appears to be less restrictive than the criterion for inflection point instability, particularly if the air has weak stable stratification. This points to K-H instability as the most important shear instability mechanism for development of turbulence in such cases. However, observations indicate that CAT on the cyclonic side of jet streams typically occurs in a synoptic-scale environment with Ri larger than Ri_*. In a case study investigated in Section 8 it is found that large CAT index values on the cyclonic side of upper-tropospheric jet streams typically occur in an environment with $Ri \approx 1$. This seems to indicate that the instability mechanism responsible for this type of CAT is inflection point instability rather than K-H instability. The necessary, but insufficient condition for the former type of instability is fulfilled at points (or lines) where the vertical component of shear vorticity has a local maximum. This maximum is located on the cyclonic shear side of the jet.

There are also inflection points on the anticyclonic side of the jet, at points (or lines) where the anticyclonic shear vorticity has a local maximum. However, on synoptic scales this maximum tends to be limited by $\zeta_s \geq -f - \zeta_c$, where ζ_s and ζ_c are the vertical components of shear and curvature vorticity, respectively. If ζ_s becomes less than $-f - \zeta_c$ the flow becomes unbalanced. For this reason the synoptic-scale magnitude of ζ_s on the anticyclonic side of jet streams tends to be much smaller than the corresponding values on the cyclonic side. Consequently, the likelihood of triggering turbulence by inflection point instability appears to be small on the anticyclonic shear side of jet streams, in particular if the flow has anticyclonic curvature. Under these circumstances development of turbulence is more likely to be a result of K-H instability (triggered by gravity wave activity due to flow imbalance).

From the presentation above we expect that a turbulence index as a minimum should be able to identify flow regions with strong vertical and horizontal wind shear and also regions, where flow imbalance (and gravity wave generation) may occur.

As noted previously, the shear production due to the horizontal wind shear is often neglected in the ABL. However, in the upper tropospheric jet streams strong horizontal wind shear can give a non-negligible contribution to the shear production of E_K (and E) and (anything else unchanged) lead to higher turbulent energy levels than without significant horizontal wind shear. As pointed out turbulence may in fact originate from horizontal shear production in an inflection point instability process. The latter process can occur independently of whether or not the condition $Ri < 0.25$ is satisfied. In presence of vertical wind shear S the inflection point instability also activates vertical shear production.

4: CAT in regions with large horizontal deformation

According to the discussion above a CAT index should be able to capture the strong velocity shear regions associated with jet cores in the upper troposphere. Historically, focus has mainly been on strong velocity shear regions created by frontogenesis (e.g. review by Knox 1997). The frontogenesis function on a pressure surface, p, is defined

$$F = \frac{D}{Dt}|\nabla_p \theta_v|, \tag{3}$$

where $D/Dt = \partial/\partial t + \mathbf{V} \cdot \nabla_p$ is the material derivative. Thus the frontogenesis function, F, measures the rate of change of the magnitude of the quasi-horizontal gradient of the virtual potential temperature θ_v of an air parcel moving with the air. In a coordinate system rotated such that the shearing deformation $DSH = \partial v/\partial x + \partial u/\partial y$ is zero, i.e if the x-axis is either along the axis of dilatation ($DST > 0$) or the axis of contraction ($DST < 0$), the horizontal frontogenesis function can be written in the form (e.g. Bluestein 1993)

$$F = 1/2|\nabla_p \theta_v|(DST \cos 2\alpha - DIV), \tag{4}$$

where $DST = \partial u/\partial x - \partial v/\partial y$ is the stretching deformation, $DIV = \partial u/\partial x + \partial v/\partial y$ is the horizontal divergence and α is the angle from the x-axis (after rotation) to the θ_v isolines. It can be noted that DST acts frontogenetically/ frontolytically if the axis of dilatation/contraction is along the x-axis ($DST > 0/DST < 0$) and $|\alpha| < 45°$.

The most widely used CAT index in the past is perhaps that suggested by Ellrod and Knapp (1992). This dimensional (s^{-2}) index is defined

$$TI2 = S(DEF - DIV), \tag{5}$$

where $DEF = (DSH^2 + DST^2)^{1/2}$ is the total deformation, i.e. the magnitude of the horizontal deformation. Based on the observation that DIV often is much smaller than DEF they also defined another index, $TI1$, obtained by neglecting DIV in (5). The $TI2$ index is derived directly from (4), by applying optimal conditions for frontogenesis, i.e. $\alpha = 0°/\alpha = 90°$ and $DST > 0/DST < 0$, and using the thermal wind equation to replace $|\nabla_p \theta_v|$ with the magnitude of the vertical shear of the horizontal wind. Since (4) is valid in a coordinate system with the x-axis along either the axis of dilatation or contraction it follows that $DSH = 0$ and therefore $DEF = |DST|$. This implies that high values of $TI2$ may also occur in regions of frontolysis. Unless CAT is not very sensitive to whether wind shears increase or decrease with time, this points to an inherent risk of false alarms of CAT in the latter regions, when (5) is used as a CAT predictor.

A jet streak, which is a wind maximum in the jet core, may serve to illustrate the difference between(4) and (5). Consider a case, where $\alpha = 0$ (streamlines parallel to isotherms), which is the optimal frontogenesis/frontolysis situation. In the entrance/exit region of the jet streak $DST > 0/DST < 0$, which means frontogenesis ($F > 0$)/frontolysis ($F < 0$) due to flow deformation in the entrance/exit region, but (5) predicts high values of $TI2$ in both the entrance and exit region. In other words, $TI2$ is able to recognize a jet streak, but unable to distinguish between the entrance and exit regions of jet streaks.

According to the discussion in Section 3 the relative success and widespread use of $TI2$ is probably related to its ability to identify regions with a local maximum in shear vorticity on the cyclonic side of jet streams. These regions are also frontal zones with larger vertical wind shear S and higher static stability N^2 than is typical for the surrounding tropospheric air masses (e.g. Figure 10.4a in Shapiro and Keyser 1990).

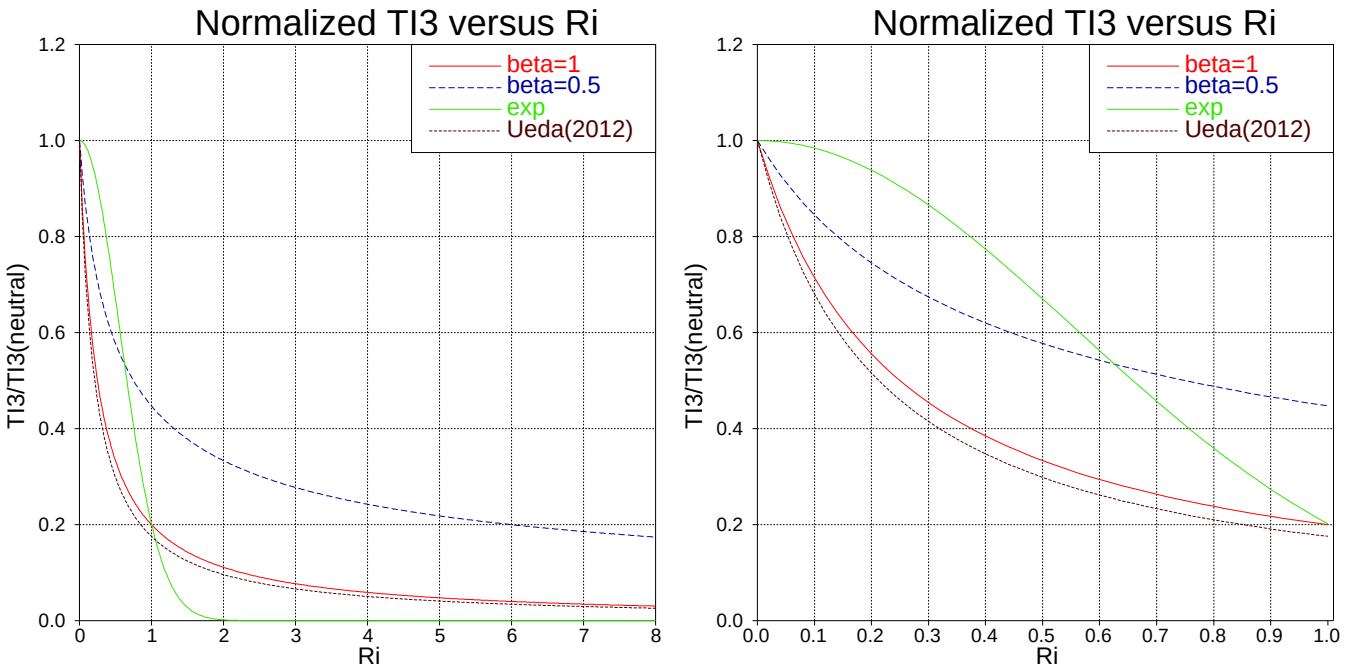

Figure 1: CAT index $TI3$ normalized by its neutral value as function of the gradient Richardson number Ri. Curves are for $\beta = 1, \beta = 0.5$ and for alternative stability functions $\exp(-0.1\chi^{-2})$ (exp) and $(1 + 4.7Ri)^{-1}$ (Ueda et al. 2012). The figure to the right is an enlargement of the left figure with a cut-off at $Ri = 1.0$.

5: A DMI-HIRLAM CAT (clear air turbulence) index for flow with substantial deformation

$TI2$ defined in (5) does not contain any effect of stratification of the air, usually measured by N^2. However, as indicated by the arguments below, it appears plausible that CAT also ought to be dependent on N^2. Consider for example a flow having a time independent vertical wind shear S, but a static stability N^2 increasing with time. For this flow Ri increases with time, and according to Figure 3a in Zilitinkevich et al. (2007) the non-diagonal Reynolds stresses representing the vertical fluxes of momentum ($\overline{u'w'}$ and $\overline{v'w'}$) decrease with increasing Ri. It then follows from the second term on the r.h.s of (1) that the shear production of E_K due to vertical wind shear also decreases with increasing Ri. Under these circumstances, including possible contribution from non-negligible horizontal shear production, the expectation is that E_K as well as E decreases as Ri increases. The following dimensionless CAT index, applied for $N^2 \geq 0$, is proposed:

$$TI3 = \frac{TI2}{N_0^2}(1 - (1 + \frac{N_*^2}{N^2})^{-1}) = \frac{TI2}{N_0^2}(\frac{\chi}{1+\chi})^{\beta}, \tag{6}$$

where $\chi = Ri_*/Ri$, $Ri_* = 0.25$, $N_*^2 = Ri_* S^2$ and $N_0^2 = 10^{-7}\, s^{-2}$. The latter makes $TI3$ nondimensional and re-scales the index such that it in neutral stratification becomes equal to 1 for $S = 10^{-2}\, s^{-1}$, and $DEF = 10^{-5}\, s^{-1}$. The latter are typical order of magnitude values for mid-latitude synoptic-scale flow in baroclinic regions of the troposphere. Ri_* is the critical value below which K-H instability becomes possible. Tentatively, we have chosen $\beta = 1$. In neutral to weakly stable stratification ($0 \leq Ri << Ri_*$) $TI3$ can then be approximated by

$$TI3 \approx \frac{TI2}{N_0^2} \tag{7}$$

and in strongly stable stratification ($Ri >> Ri_*$) the approximation becomes

$$TI3 \approx \frac{TI2}{N_0^2}\chi(1-\chi). \tag{8}$$

The variation of $TI3$ normalized by its neutral value as function of Ri is depicted in Figure 1 (the curve marked beta=1). At the critical gradient Richardson number Ri_* the index is 50 percent of its neutral value. Three alternative $TI3$ indices with other stability dependencies are also shown in Figure 1. These curves, except the curve marked Ueda(2012) are discussed in some details in Section 8. Incidentally the stability dependence of $TI3$ given by (6) is close to the stability dependence of the eddy exchange coefficient K_m normalized by its neutral value K_{mn} found by Ueda et al. (2012) to be $K_m \cdot Kmn^{-1} = (1 + 4.7Ri)^{-1}$. The eddy exchange coefficients were measured in the upper troposphere to lower stratosphere by a middle and upper atmosphere very high frequency Doppler radar. Measurements were done in clear air and with exclusion of cases with horizontal wind speeds larger than $40\,m\,s^{-1}$.

As noted previously, in jet streams having strong vertical and horizontal velocity shear, the air is usually stably stratified, and therefore large positive $TI3$ points to regions, where CAT due directly to shear instability (i.e. not shear instability resulting from gravity wave activity generated by other instability mechanisms) is likely to occur.

In an observational study of a representative sample of severe turbulence cases (7 out of a total of 44) Kaplan et al. (2005) noted that all these cases occurred relatively close to a minimum value in the vertical variation of Ri, but they also found that Ri was not among the 12 most important predictors of severe turbulence in the 44 cases they investigated. Also other investigators of CAT found rather poor correlation between Ri and occurrence of CAT (e.g. Dutton and Panofsky 1970).

These observations are not necessarily in disagreement with (6), despite of the fact that $TI3$ at a given value of $TI2$ does decrease with increasing Ri. Large uncertainties in estimates of Ri are likely to contribute to the reported weak correlation between Ri and observed CAT.

6: CAT in regions with small horizontal deformation

For flow in gradient-wind balance the relation between DEF, $\zeta = \partial v/\partial x - \partial u/\partial y$ (relative vorticity), and DIV is

$$DEF^2 = \zeta^2 + DIV^2 - 4J(u,v), \tag{9}$$

where $J(u,v) = \partial u/\partial x \cdot \partial v/\partial y - \partial v/\partial x \cdot \partial u/\partial y$ is the Jacobian operator. For flow in gradient-wind balance $\zeta = \zeta_s + \zeta_c$, where $\zeta_s = -\partial V/\partial n$ is the shear vorticity and $\zeta_c = V/R$ is the curvature vorticity. R is the radius of curvature of the streamlines and n is the direction of the normal vector, which points to the left of the flow direction. (Holton 2004). Further $J(u,v) = \zeta_s\zeta_c$ (Knox 1997). Substitution of ζ_s and ζ_c in (9) gives

$$DEF^2 = (\zeta_s - \zeta_c)^2 + DIV^2. \tag{10}$$

Equation (10) implies $DEF \geq |DIV|$, and if $DEF >> |DIV|$, which is usually the case for flow on synoptic scales, we have $DEF \approx |\zeta_c - \zeta_s|$, showing that DEF and $TI2$ become small if $\zeta_c \approx \zeta_s$ regardless of the magnitude of ζ_s.

The role of the divergence is to reduce and enhance $TI2$ if the divergence is positive and negative (convergence), respectively. As noted above DIV has usually little influence on the magnitude of $TI2$ on synoptic scale, since it tends to be an order of magnitude smaller than DEF. In fact, in the quasi-geostrophic framework (a reasonable approximation for flow on synoptic scales outside the

equatorial region) the quasi-geostrophic wind is non-divergent. If such a flow has divergence, the divergence is in the ageostrophic part of the flow. For a given magnitude of the vertical wind shear it then follows from (5) that $TI2$ becomes small if DEF is small, and according to (10) the latter is small if $\zeta_c \approx \zeta_s$, regardless of the magnitude of ζ_s. Consequently, $TI2$ is small for a flow with large vertical and horizontal velocity shear (the latter given by ζ_s) and large curvature (since we consider the case $\zeta_c \approx \zeta_s$). However, development of turbulence by dynamic instability also appears likely in such flow conditions. This calls for a CAT index giving high values for the flow conditions just described and small values in cases, where DEF is large.

6.1: Vertical wind shear

Large vertical shear of the geostrophic wind is created in baroclinic zones of the atmosphere. These zones are frontal regions separating air masses of widely different origin. If the flow has curvature the wind field is closer to be in gradient than geostrophic wind balance. Following Palmén and Newton (1963)

$$\frac{\partial V}{\partial z} = f\frac{\partial V_g/\partial z}{f+2\zeta_c} + \frac{{\zeta_c}^2 \partial R/\partial z}{f+2\zeta_c}, \tag{11}$$

and Knox (1997)

$$\frac{\partial V_a}{\partial z} = \frac{-2\zeta_c \partial V_g/\partial z}{f+2\zeta_c} + \frac{{\zeta_c}^2 \partial R/\partial z}{f+2\zeta_c}. \tag{12}$$

In (11) and (12) V is the gradient wind, V_g the geostrophic wind and $V_a = V - V_g$ the ageostrophic wind. In the case $\zeta_s = \zeta_c$ the denominators in (11) and (12) become $f + \zeta = \eta$, where η is the absolute vorticity. Consider, for the purpose of illustration, a circulation L with cyclonic curvature vorticity and a circulation H with anticyclonic curvature vorticity, both with $\zeta_s = \zeta_c$. Assume for simplicity that the circulations have the same numerical value of ζ, the same $\partial V_g/\partial z$ and $\partial R/\partial z = 0$. Then if $\zeta_L = cf = -\zeta_H$ and $0 < c < 1$, the ratio of the vertical wind shear in the anticyclonic and cyclonic circulation becomes

$$(\partial V/\partial z)_H/(\partial V/\partial z)_L) = (1+c)/(1-c), \tag{13}$$

showing that even in the presence of a rather weak vertical geostrophic wind shear, the vertical shear of the gradient wind in the anticyclonic circulation H becomes large if c is close to 1, i.e. if the absolute vorticity $\eta = f + \zeta$ approaches zero.

Atmospheric flow on synoptic scales usually satisfies the condition $\eta \geq 0$, and it has been shown (e.g. Markowski and Richardson 2010) that $\eta < 0$ is a necessary but insufficient condition for pure inertial instability. The latter results in development of gravity waves in connection with geostrophic adjustment (e.g. Vallis 2006), or, according to the Lighthill-Ford theory, by spontaneously emitted inertia-gravity waves (Knox et al. 2008). Triggering of turbulence (CAT) by gravity waves thus appears to be possible in strongly anticyclonic regions of zero or negative absolute vorticity. These regions have $\zeta_c \approx -0.5f$ and $\zeta_s \approx \zeta_c$, but as discussed previously, $TI2$ is small in such cases since DEF is small. $TI2$ is also small if $\zeta_c \approx \zeta_s > 0$, but in such cases the flow is balanced and if CAT develops it has been argued that it most likely originates from inflection point instability, which requires substantial horizontal and vertical wind shear. If the vertical gradient of the radius of curvature is zero (11) shows that at a fixed vertical shear of the geostrophic wind the corresponding gradient-wind shear decreases with increasing cyclonic curvature vorticity. Since we are considering a case with $\zeta_c \approx \zeta_s$ the shear vorticity increases, while the vertical wind shear decreases. Therefore it is most likely that the probability of CAT decreases or remains more or less unchanged if the cyclonic curvature vorticity increases.

7: A DMI-HIRLAM CAT (cloudy air turbulence) index for flow with little or no deformation

The denominator in (11) and (12) can be written $f + 2\zeta_c = \eta + (\zeta_c - \zeta_s)$. According to (10) $(\zeta_c - \zeta_s)^2 = DEF^2 - DIV^2$. This suggests that $1/\epsilon$, where $\epsilon = \eta + |\zeta_c - \zeta_s|$, could be a usable part of a CAT index for the anticyclonic shear regions of anticyclonically curved flow. If ϵ becomes small the vertical wind shear becomes large and enhances the probability of K-H instability. If ϵ becomes zero or negative the flow becomes unbalanced, which can lead to development of CAT triggered by gravity waves. Since gravity waves do not develop if the air is neutral or unstably stratified ($N^2 \leq 0$), it is expected that a CAT index applied for the anticyclonic side of jet streams must contain a measure of the static stability of the air. On the other hand it is not expected that turbulence generated by gravity waves can be sustained with high intensity if the air is strongly stratified.

Based on the just presented arguments the following CAT index, appropriate in flow regimes with weak DEF and applied for $N^2 \geq 0$, is suggested: If $N^2 \geq 0$

$$TI4 = \frac{\zeta^2}{\epsilon^2}\left(1. - (1. + \frac{N_*^2}{N^2})^{-1}\right) = \frac{\zeta^2}{\epsilon^2}\left(\frac{\chi}{1+\chi}\right)^{\beta}. \tag{14}$$

Otherwise $TI4 = 0$. It has been assumed that $TI4$ has the same dependence on Ri as $TI3$.

7.1: Discussion of the properties of the TI4 index

It follows from the definition of ϵ that this parameter becomes zero if $\zeta = \zeta_0$, where $\zeta_0 = -f - \sqrt{DEF^2 - DIV^2} \leq -f$ in the Northern Hemisphere (NH) and $\zeta_0 = -f + \sqrt{DEF^2 - DIV^2} \geq -f$ in the Southern Hemisphere (SH). The following discussion will be for NH, i.e. for $f > 0$. If $\sqrt{DEF^2 - DIV^2} > 0$, ϵ is minimized for an unbalanced flow, since $\zeta_0 < -f$, and as the total deformation $\sqrt{DEF^2}$ increases, the minimization occurs in increasingly unbalanced flow conditions. In the following two subsections we discuss the factor ζ^2/ϵ^2 in some details.

7.2: Anticyclonic flow in the Northern Hemisphere

Consider an anticyclonic flow with $\zeta = \gamma f$ ($\gamma < 0$) and $\zeta_s = a\zeta$. Then if $a \leq 0.5$

$$\epsilon = f(1 + 2a\gamma) \tag{15}$$

$$\frac{\zeta^2}{\epsilon^2} = \frac{\gamma^2}{(1+2a\gamma)^2} \tag{16}$$

and if $a \geq 0.5$

$$\epsilon = f(1 + 2(1-a)\gamma) \tag{17}$$

$$\frac{\zeta^2}{\epsilon^2} = \frac{\gamma^2}{(1+2(1-a)\gamma)^2}. \tag{18}$$

In the interval $0 < a \leq 0.5$ the parameter ϵ becomes zero if $\zeta = -f/(2a)$, and in the interval $0.5 \leq a < 1$ ϵ becomes zero if $\zeta = -f/(2(1-a))$. The parameter ϵ^2 is larger than zero for any other value of a. Note that for $a = 0$ the flow only has anticyclonic curvature vorticity, and for $a = 1$ it only has anticyclonic shear vorticity. These flow types have $\zeta^2/\epsilon^2 = \gamma^2$. According to (16) and (18) $\zeta^2/\epsilon^2 < \gamma^2$ if $a < 0$, which is the cyclonic shear side of flow with anticyclonic curvature, or $a > 1$, which is the anticyclonic shear side of flow with cyclonic curvature. If $0 < a < 1$ we have

$\zeta^2/\epsilon^2 > \gamma^2$. The factor ζ^2/ϵ^2 approaches infinity as ζ approaches $-f/(2a)$ if $0 < a \leq 0.5$ (flow with anticyclonic curvature vorticity larger than or equal to the anticyclonic shear vorticity) and $-f/(2(1-a))$ if $0.5 \leq a < 1$ (for flow with anticyclonic shear vorticity larger than or equal to the anticyclonic curvature vorticity). We note that if a is close to either 0 or 1 the negative relative vorticity at which $\epsilon = 0$ becomes numerically much larger than f.

In summary it can be stated that ζ^2/ϵ^2 becomes very large only if $a \approx 0.5$, and approaches 1 for $\gamma << -1$. In the special case $a = 0.5$ ($\zeta_c = \zeta_s < 0$) we have $\zeta^2/\epsilon^2 = \gamma^2/(\gamma-1)^2$, becoming infinity if $\gamma = -1$, i.e. if $\zeta = -f$.

7.3: Cyclonic flow in the Northern Hemisphere

In a cyclonic flow ($\zeta = \gamma f, \gamma > 0$) we get for $a \leq 0.5$

$$\epsilon = f(1 + 2(1-a)\gamma) \tag{19}$$

$$\frac{\zeta^2}{\epsilon^2} = \frac{\gamma^2}{(1+2(1-a)\gamma)^2} \tag{20}$$

and for $a \geq 0.5$

$$\epsilon = f(1 + 2a\gamma) \tag{21}$$

$$\frac{\zeta^2}{\epsilon^2} = \frac{\gamma^2}{(1+2a\gamma))^2}. \tag{22}$$

Equation (20) and (22) show that $\epsilon \geq f(1+\gamma) > 0$. The minimum value $\epsilon = f(1+\gamma)$ occurs for $a = 0.5$. In contrast to the anticyclonic flow this minimum can not be zero, since $\gamma > 0$. For the same value of a and the same $|\zeta|$ we obtain $\epsilon_{af} - \epsilon_{cf} = -2|\zeta|$, where ϵ_{af} and ϵ_{cf} are for the anticyclonic and cyclonic flow, respectively. Under these conditions the factor ζ^2/ϵ^2 is therefore always largest for the anticyclonic flow.

7.4: Summary of section 7

The discussion given in the last two subsections shows that the factor ζ^2/ϵ^2, which is an important part of the $TI4$ index, becomes large on the anticyclonic shear side of anticyclonically curved flow and very large if $\eta \approx 0$. Otherwise the factor is relatively small, particularly in flow with large $|a|$ and $|\gamma|$. Since $(\zeta_s - \zeta_c)^2 = (\gamma f(2a-1))^2$ it follows from (10) that this type of flow has large total deformation, and the appropriate CAT index should therefore be $TI3$ (or $TI2$).

The $TI4$ index mainly points to midlatitude regions of the flow where $a \approx 0.5$. If a is equal to or a little higher than 0.5, CAT can develop by shear instability due to a large horizontal and vertical wind shear (11). If CAT is less than 0.5, CAT can develop by K-H instability triggered by modulation of the vertical wind shear by gravity waves generated by the unbalanced flow. $TI4$ becomes infinity if $\epsilon = 0$. For practical use $TI4$ has therefore been rescaled by the factor $(1 + \zeta_*/\epsilon^2)^{-1}$, where $\zeta_* = cf$. Equation (14) then reads

$$TI4 = \frac{\zeta^2}{\epsilon^2}\left(1 + \frac{\zeta_*^2}{\epsilon^2}\right)^{-1}\left(\frac{\chi}{1+\chi}\right)^{\beta}. \tag{23}$$

We have chosen $c = 0.1$ such that ζ_* is a typical magnitude of the relative vorticity on synoptic scales. In the case $\zeta_s = \zeta_c$, corresponding to $a = 0.5$, the index becomes $TI4 = (c^2 + ((1+\gamma)/\gamma)^2)^{-1} \cdot \chi^{\beta}(1+\chi)^{-\beta}$ and for $\zeta = -f$ the index is $TI4 = c^{-2} \cdot \chi^{\beta}(1+\chi)^{-\beta}$. If ζ becomes substantially less than $-f$, which may happen on sub-synoptic scales, $TI4$ is smaller

than in cases where $\zeta \approx -f$. Therefore $TI4$ is not expected to be an appropriate CAT index for sub-synoptic scale flow having a relative vorticity substantially less than $-f$. However, by modifying the index such that it reads

$$TI4_m = \frac{\zeta^2}{(\zeta_0 - \zeta)^2 + \zeta_*^2} \left(\frac{\chi}{1+\chi} \right)^{\beta} \tag{24}$$

it attains a maximum for $\zeta = \zeta_0$ instead of for $\zeta = -f$. ζ_0 has been defined in Section 7.1 as the relative vorticity at which $\epsilon = 0$. $TI4$ and $TI3(TI2)$ are complementary in the sense that $TI4$ is large and $TI2$ small if DEF is small and vice versa if DEF is large. This behavior is consistent with Sparks et al. (1977) and Knox (1997), both arguing for a nonlinear relationship between CAT and absolute vorticity, with a maximum of CAT at $\zeta + f \approx 0$ (small DEF) and another maximum when $\zeta + f >> 0$ (large DEF).

8: Case studies

The following example serves to demonstrate the behavior of the proposed two CAT indices. A verification against CAT observations has not been done due to difficulties in getting access to pilot reports of CAT. The presented CAT indices are therefore experimental and need to be verified (and if necessary modified) before possible operational use. Figure 2 shows DMI-HIRLAM-T15 6 hour forecasts of $TI3$ and $TI4_m$ at model-level 15 (approximately at 9 km height) valid at 12 UTC on 1 December 2011. The model has 40 unequally spaced vertical levels, more closely packed near the surface than aloft, and a horizontal resolution of approximately 15 km. The stability function $F_1 = \chi \cdot (1+\chi)^{-1}$ has been applied in Figure 2 (top) and in Figure 2 (bottom) the applied stability function is $F_2 = \exp(-0.1\chi^{-2}) = \exp(-1.6Ri^2)$. To suppress high values of the indices close to the ground they have been multiplied with $V_h/30^2$ at horizontal wind speeds below $30\, m\, s^{-1}$. It can be seen from Figure 1 that $TI3$ calculated by using F_1 is less/larger than $TI3$ based on F_2 if $Ri < 1/Ri > 1$. By intercomparison of Figure 2 (top) and Figure 2 (bottom) it can be noted that the regions with $TI3 > 0.6$ become smaller when F_2 is applied, and it can also be seen that the maximum values tend to be a little higher. Therefore Ri within regions where $TI3 > 0.6$ (Figure 2, top) is close to 1 with minimum values a little less than 1 in the cores and values a little higher than 1 in the outer part of the regions. In contrast values of $TI4_m > 0.6$ generally decrease when F_1 is replaced by F_2. This is most clearly seen in Figure 3. The latter figure is similar to Figure 2, but for model-level 12 (approximately at 12 km height). The values of Ri within the regions where $TI4_m > 0.6$ must therefore be somewhat larger than 1. Another formulation with the stability function given by $F_3 = \exp(-0.1N^2 \cdot N_0^{-2})$ has also been applied. With the latter formulation $TI3$ was nowhere above 0.6, while the regions with $TI4_m > 0.6$ expanded somewhat (figures not shown). This result shows that $N_a^2 < N_c^2$ in regions with high values of the indices. The subscripts a and c refer to the anticyclonic and cyclonic side of jet streams, respectively. Combined with the previous result $Ri_a > Ri_c$ we can also conclude for vertical wind shear that $S_a < S_c$ in the considered regions. These results fit nicely with the typical synoptic-scale distribution of static stability and vertical wind shear in upper-tropospheric jet streams as depicted in Figure 10.4a in Shapiro and Keyser (1990). The frontpage figure shows results for the indices if the stability function $\chi^{1/2}(1+\chi)^{-1/2}$ is applied, corresponding to $\beta = 0.5$ in Figure 1.

Previously it has been argued that K-H instability seems to be the most common instability mechanism leading to CAT in the stably stratified environment on the anticyclonic side of jet streams. However, the regions depicted by $TI4_m$ in the case under investigation have $Ri > 1$. In order to generate turbulence one or more processes that are able locally (on a sub-synoptic scale) to create $Ri < Ri_*$ must be activated. It was mentioned in the introduction that such processes could be initiated in unbalanced flow. Gravity waves produced by geostrophic adjustment (e.g. Vallis 2006)

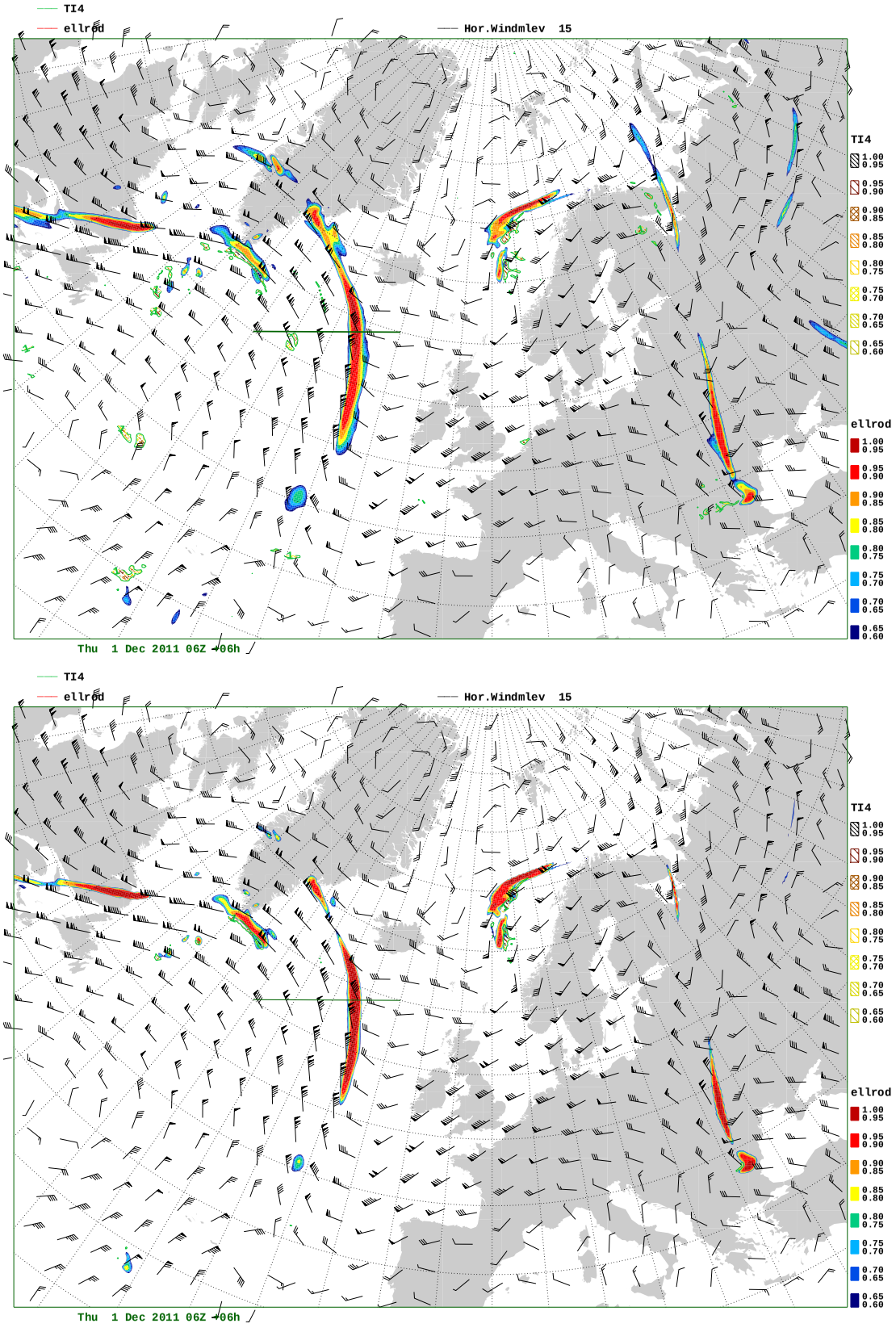

Figure 2: 6 hour forecasts of CAT index $TI3$ and $TI4_m$ at model-level 15 (height: approximately 9 km) valid at 12 UTC on 1 December 2011. (Top) with stability function F_1 and (bottom) with stability function F_2. $TI3$ is shown by blue to dark red colors, and $TI4_m$ by hatched colors (yellow to dark red). Only index values ≥ 0.6 are shown. Green contour for $TI4_m$ is 0.6. Vertical cross sections in Figure 4 are along the line from 35w-55n to 15w-60n. The indices have been scaled to values between 0 and 1 by $1 - \tanh(TI3^{-1})$ and $1 - \tanh(2TI4^{-1})$, respectively.

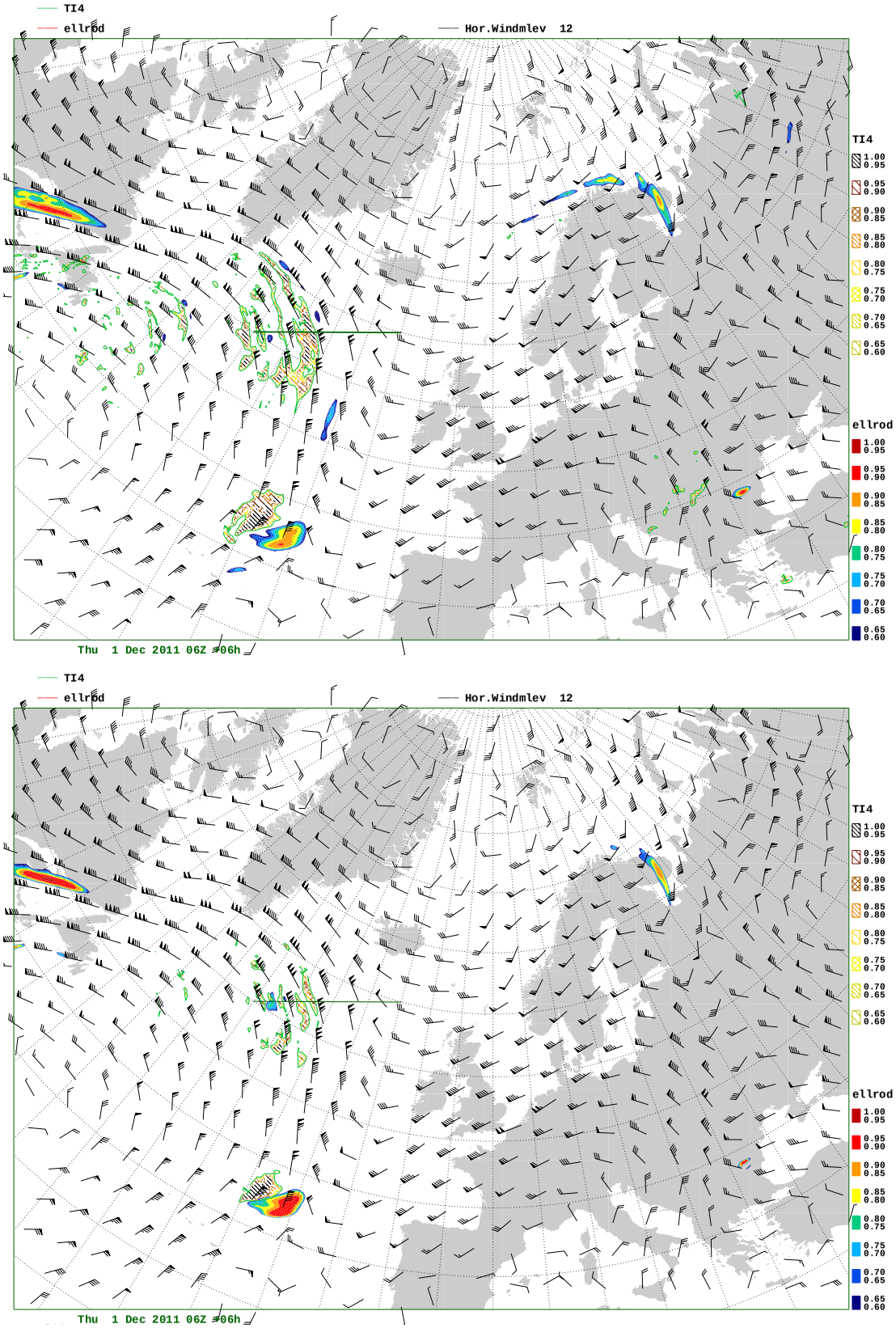

Figure 3: Same as Figure 2, but for model-level 12 (height: approximately 12 km).

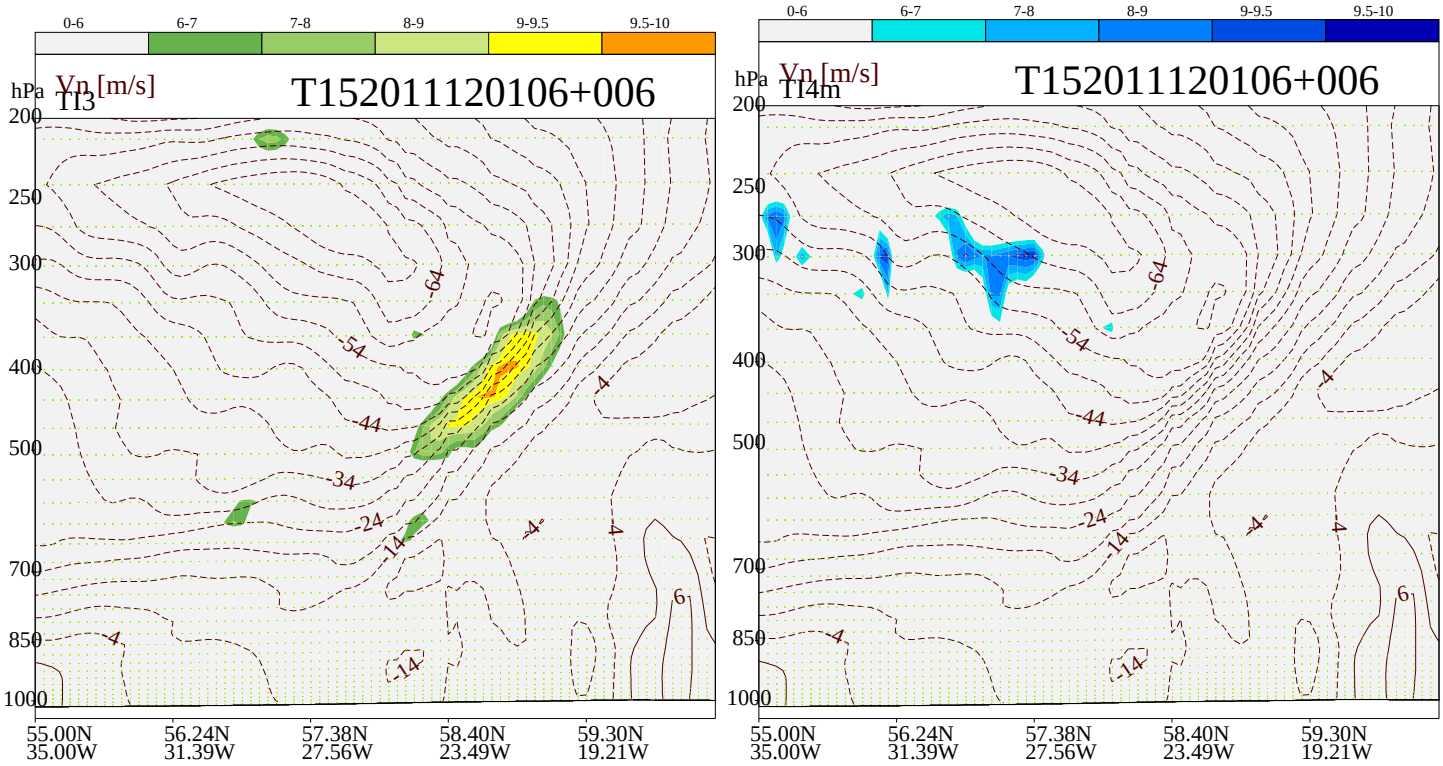

Figure 4: Vertical cross sections along the line marked in Figure 2, showing 6 hour forecasts of $TI3$ (left) and $TI4_m$ (right) valid at 12 UTC 1 December 2011. Values shown by color bars at top of figure. Note that the indices have been multiplied by 10. Wind speed normal to the cross section shown by dashed lines at $5\,m\,s^{-1}$ intervals, negative for flow out of the plane.

and spontaneously emitted gravity waves (e.g. Knox et al. 2008) have been proposed as possible mechanisms. In $TI4_m$ the vorticity term $\zeta^2((\zeta_0-\zeta)^2+\zeta_*^2)^{-1}$ points to regions where the flow is likely to be unbalanced. The stability function is identical with that for $TI3$. Since CAT may develop by different processes on the cyclonic and anticyclonic side of jet streams there is no obvious reason why the stability functions should be identical. However, it appear plausible that $TI4_m$ should increase with decreasing N^2, since larger amplitude of the gravity waves and associated stronger modulation of the wind is expected to occur if N^2 is decreased.

Figure 2 and 3 (and other cases not presented) show quite clearly that large values of $TI3$ and $TI4_m$ have little overlap. It is also a common feature that the index-fields, and in particular $TI4_m$, look more noisy on the anticyclonic side of the jet streams. This seems to be related to a tendency of the model to have more small-scale flow patterns on the anticyclonic side, where stratiform cloud layers, often with embedded DMC, usually are present. The spatial separation of the indices is in good agreement with the analysis presented in Section 7. In the vertical cross section in Figure 4 the spatial separation of the indices is also evident. It can be noted that the horizontal shear of the wind component normal to the cross section is substantially larger in the frontal zone, where $TI3$ has high values, than on the anticyclonic side of the jet, where spots of high values of $TI4_m$ are found in a zone with relatively large vertical wind shear.

The $TI3$ index has regularly been compared with the CAT-index presented in significant weather maps on opmet.dmi.dk and good agreement has generally been found. It has turned out to be much more difficult to evaluate the index $TI4_m$. So far we only have one report of severe turbulence on the anticyclonic side of a jet stream. This case is shown in Figure 5. The reported turbulence was at flight-level 390 (11.7 km) at the black dot in Figure 5 (bottom). The model (at 6 UTC) failed to

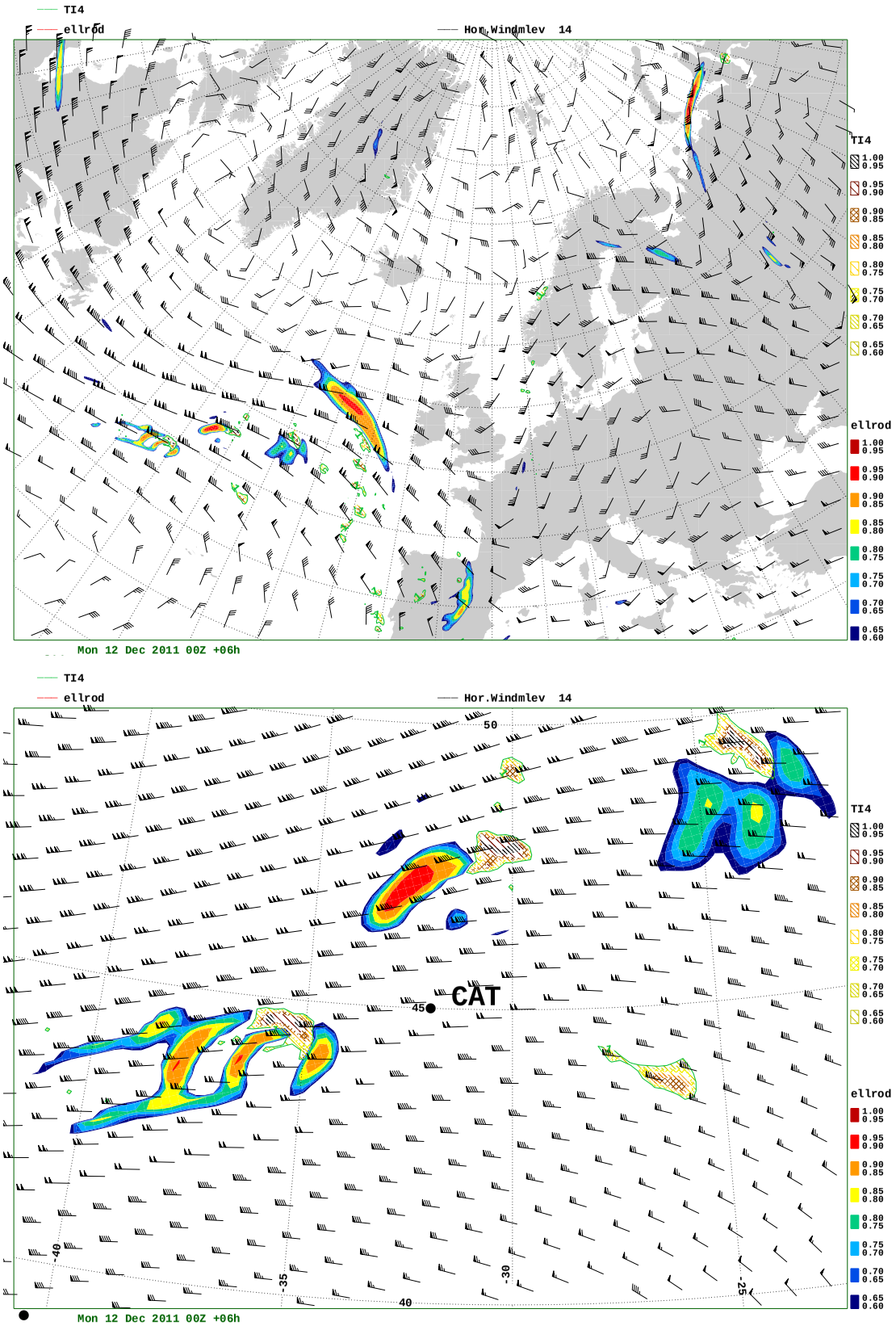

Figure 5: As Figure 2, but for 6 hour forecasts of CAT index $TI3$ and $TI4_m$ (using stability function F_1) at model-level 14 (height: approximately 10 km) valid at 06 UTC on 12 December 2011. Bottom figure zooms in on a region near the Azores on the anticyclonic shear side of a southwesterly jet over the central North Atlantic. The black dot shows approximate location where CAT was reported at 0653 UTC. Otherwise as Figure 2.

predict turbulence at the report-location, but had spots of high index-values of $TI3$ and $TI4_m$ within horizontal distances of about 200 km from the observation and 1 to 2 km below the flight-level. The latter result is not convincing and illustrates the need for verification of the proposed indices, not least $TI4_m$.

Conclusions

Two dimensionless CAT indices valid for midlatitude synoptic-scale flow in the upper troposphere have been presented. The indices ($TI3$ and $TI4/TI4_m$) are applicable to flow with high and low resultant horizontal deformation, respectively. It was argued that the $TI3$ type of turbulence mainly originates from inflection point instability in the horizontal flow, while the $TI4$ type mostly originates from K-H instability triggered by gravity wave activity in unbalanced flow. Both indices are functions of static stability, which is a novel feature compared to most CAT indices documented in the literature. Preliminary results indicate that Ri has a local minimum close to 1 in regions with high values of the indices, and with a tendency for Ri to be highest in regions where $TI4/TI4_m$ is high. The TI3 index is related to the indices $TI1$ and $TI2$ proposed by Ellrod and Knapp (1992). The $TI4/TI4_m$ indices are alternatives to a horizontal divergence trend term proposed by Ellrod and Knox (2005). The former indices point to regions on the anticyclonic side of jet streams, where the flow is likely to be unbalanced. Vertical wind shear (in frontal zones with large horizontal wind shear) and total horizontal deformation are key parameters in $TI3$. In $TI4/TI4_m$ the key parameter is relative vorticity. The proposed post-processed indices are so far experimental products. Possible operational use of the indices must wait for a thorough verification of the indices (and in particular $TI4/TI4_m$) against CAT reports.

References

[H. B. Bluestein 1993] Synoptic-Dynamic Meteorology in Midlatitudes. Vol. 2: Observations and Theory of weather systems. Oxford University Press, p. 431-432.

[J.A. Dutton and H.A. Panofsky 1970] Clear air turbulence: A mystery may be unfolding. Science, 167, 937-944.

[G. P. Ellrod and J. A. Knox 2005] An improved clear air turbulence diagnostic index to account for unbalanced flow in anticyclonically curved jet streams. 21st Conference on Weather Analysis and Forecasting/17th Conference on Numerical Weather Prediction, 8pp.

[G. P. Ellrod and D. J. Knapp 1992] An objective clear-air turbulence forecasting technique: Verification and operational use. Wea. Forecasting, 7, 150-165.

[J. R. Garratt 1994] The atmospheric boundary layer. Cambridge atmospheric and space science series, Cambridge University Press.

[J. R. Holton 2004] An introduction to dynamic Meteorology, fourth edition. ELSEVIER Academic Press.

[J.M. Fritsch and R.A. Maddox 1981] Convectively driven mesoscale weather systems aloft. Part 1: Observations. J. Appl.Meteor., 20, 9-19.

[J. A. Knox, 1997] Possible Mechanisms of Clear-Air Turbulence in Strongly Anticyclonic Flows. Mon. Wea. Rev, 125, 1251-1259.

[J. A. Knox, D. W. McCann, and P. D. Williams 2008] Application of the Lighthill-Ford Theory of Spontaneous Imbalance to Clear-Air Turbulence Forecasting. J. Atmos. Sci., 65,3292-3304.

[M.L. Kaplan, A.W. Huffman, K.M. Lux, J.J. Charney, A.J. Riordan, and Y.-L. Lin 2005] Characterizing the severe turbulence environments associated with commercial aviation accidents. Part 1: A 44-case study synoptic observational analyses. Meteorol. Atmos. Phys., 88, 129-152.

[E. Palméen and C. W. Newton 1963] Atmospheric Circulation Systems. Their Structure and Physical Interpretation. Academic Press. International Geophysics Series, Vol. 13, p. 223.

[M.A. Shapiro and D. Keyser 1990] Fronts, Jet Streams and the Tropopause. Extratropical Cyclones: The Erik Palmén Memorial Volume, Eds. C.N. Newton and E.O. Holopainen, 167-191.

[W.R. Sparks, S.G.Cornford, and J.K. Gibson 1977] Bumpiness in clear air and its relation to some synoptic-scale indices. Geophysical Memoirs 121, 53 pp. [Available from U.K. Meteorological Office, United Kingdom].

[H. Ueda, T. Fukui, M. Kajino, M. Horiguchi, H. Hashiguchi, and S. Fukao 2012] Eddy Diffusivities for Momentum and Heat in the Upper Troposphere and Lower Stratosphere Measured by MU Radar and RASS, and a Comparison of Turbulence Model Predictions. J. Atmos. Sci., 69, 323-337.

[G. K. Vallis 2006] Atmospheric and Ocean Fluid Dynamics. Fundamentals and Large-Scale Circulation. Cambridge University Press, 144-152.

[S. S. Zilitinkevich, T. Elperin, N. Kleeorin and I. Rogachevskii 2007] Energy- and flux-budget (EFB) turbulence closure model for stably stratified flows. Part 1: Steady-state, homogeneous regimes. Atmospheric Boundary Layers: Nature, Theory, and Application to Environmental Modelling and Security. A. Baklanov and B. Grisogono (Eds.) Springer Science-Business Media, 11-35.

[S. S. Zilitinkevich, I. N. Esau, N. Kleeorin, I. Rogachevski and R. D. Konznetsov 2010] On the Velocity Gradient in Stably Stratified Sheared Flows, Part 1: Asymptotic Analysis and Applications. Boundary-Layer Meteorol., 125, 505-511.

Previous reports

Previous reports from the Danish Meteorological Institute can be found at:
http://www.dmi.dk/dmi/dmi-publikationer.htm